



OPEN

Surface energy-mediated construction of anisotropic semiconductor wires with selective crystallographic polarity

Jung Inn Sohn^{1*}, Woong-Ki Hong^{2*}, Sunghoon Lee^{3*}, Sanghyo Lee⁴, JiYeon Ku³, Young Jun Park³, Jinpyo Hong⁴, Sungwoo Hwang³, Kyung Ho Park⁵, Jamie H. Warner⁶, SeungNam Cha¹ & Jong Min Kim¹

¹Department of Engineering Science, University of Oxford, Oxford OX1 3PJ, UK, ²Jeonju Center, Korea Basic Science Institute, Jeonju, Jeollabuk-do 561-180, South Korea, ³Frontier Research Lab., Samsung Advanced Institute of Technology, Yongin, South Korea, ⁴Department of Physics, Hanyang University, Seoul, South Korea, ⁵Korea Advanced Nano Fab Centre, Suwon, South Korea, ⁶Department of Materials, University of Oxford, Oxford OX1 3PH, UK.

Received
10 April 2014

Accepted
19 June 2014

Published
14 July 2014

ZnO is a wide band-gap semiconductor with piezoelectric properties suitable for opto-electronics, sensors, and as an electrode material. Controlling the shape and crystallography of any semiconducting nanomaterial is a key step towards extending their use in applications. Whilst anisotropic ZnO wires have been routinely fabricated, precise control over the specific surface facets and tailoring of polar and non-polar growth directions still requires significant refinement. Manipulating the surface energy of crystal facets is a generic approach for the rational design and growth of one-dimensional (1D) building blocks^{1–4}. Although the surface energy is one basic factor for governing crystal nucleation and growth of anisotropic 1D structures, structural control based on surface energy minimization has not been yet demonstrated^{5–9}. Here, we report an electronic configuration scheme to rationally modulate surface electrostatic energies for crystallographic-selective growth of ZnO wires. The facets and orientations of ZnO wires are transformed between hexagonal and rectangular/diamond cross-sections with polar and non-polar growth directions, exhibiting different optical and piezoelectrical properties. Our novel synthetic route for ZnO wire fabrication provides new opportunities for future opto-electronics, piezoelectronics, and electronics, with new topological properties.

Correspondence and requests for materials should be addressed to S.N.C. (seungnam.cha@eng.ox.ac.uk) or J.M.K. (jong.kim@eng.ox.ac.uk)

* These authors contributed equally to this work.

Inorganic compound semiconductors with the inherent structural anisotropy continue to be of considerable interest for both fundamental science and potential technology applications due to their diverse functionalities and unique features combined with the dynamic electro-mechanical coupling and the static polarization^{10–14}. In particular, the strong electrical polarization of wurtzite semiconductors such as ZnO and GaN, arising from non-central symmetry and crystallographic polarity, has a profound effect on carrier concentration, energy band structure, photon emission energy, and excitonic behavior^{1–4}. Thus, the nature of the terminating surface on wurtzite crystal, which is intimately associated with the growth direction and the bonding state, can play a crucial role in its electrical, optical, and photophysical features. Furthermore, such anisotropic phenomena are particularly striking and relevant for one-dimensional (1D) structure due to its geometric crystal structure with the highly uniaxial anisotropy as well as the highly confined strain and polarization field, compared to bulk and film structures. Hence, tailoring facets and crystal shapes of 1D wurtzite materials through control of crystal preferred growth orientation is an effective way for achieving not only designed physical properties, but also the ability to manipulate the polarization between parallel to and perpendicular to their length. This in turn allows for creating a new concept of topological architecture and unique function pertinent to potential device applications. However, because of chemically active polar surfaces with electrostatic charges, the 1D structure of wurtzite materials typically exhibit hexagonal morphology with the strongly preferred polar growth orientation to minimize surface energy, resulting in a uniaxial polarization along the *c*-axis (growth direction)^{5,10}. As a result, it has been widely believed that it is extremely difficult to grow 1D wurtzite materials preferentially along the non-polar direction, severely limiting their use for a new topology of devices utilizing the piezoelectric field induced along the radial direction (that is, perpendicular to the growth direction) and the maximized areas of active surfaces with polarization charges.

To date, despite steadily accumulating insight into the designed physical properties through the control and inhibition of crystal growth, only a few strategies have been developed to selectively define the crystallographic

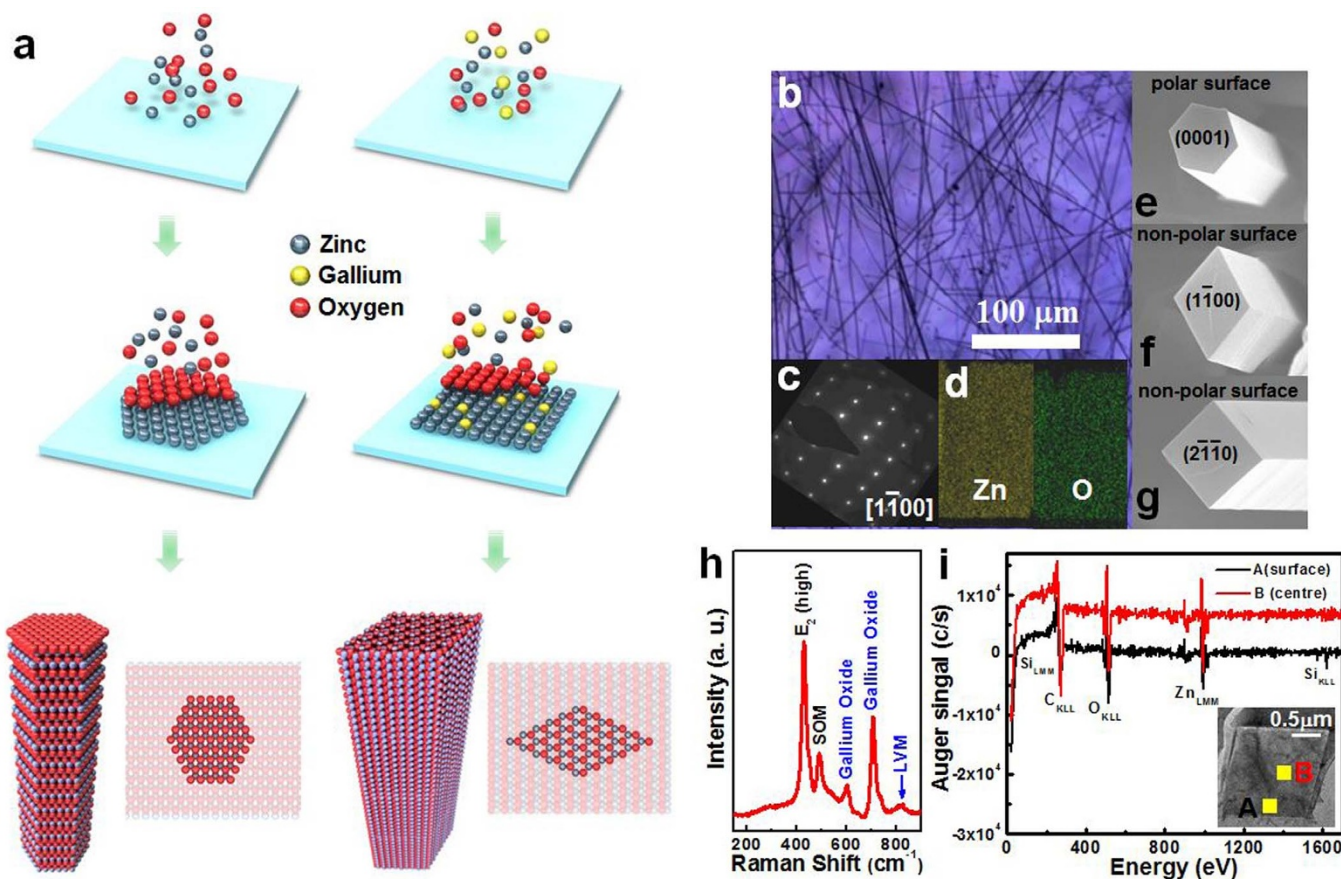


Figure 1 | Crystal structures of ZnO. (a), Schematics of different growth modes and structural models of the polar $(000\bar{1})$ and the non-polar $(10\bar{1}0)$ surfaces without and with Ga atoms replacing surface Zn atoms. The red, blue, and yellow-brown spheres indicate O, Zn, and Ga atoms, respectively. (b), Optical microscope images of ultra-long ZnO wires grown by using ZnO powder mixed with a GaAs wafer as a source material. (c, d), The SAED pattern (c) and EDS elemental mapping (d) taken from the same sample, which confirm that the wire is the wurtzite structured ZnO. (e–g), High-magnification SEM images of representative ZnO wires grown by changing the weight ratio of ZnO to GaAs sources with 20 (e), 5 (f), and 2 (g), respectively. (h), Micro-Raman spectra of a single ZnO wire with the non-polar growth direction. Additional local vibration modes, derived essentially from host lattice defects induced by dopants, were clearly observed. This indicated that Ga atoms are indicated into ZnO wires. i, FE-AES survey spectra obtained from the near surface (rectangular region marked as “A”) and centre (rectangular region marked as “B”) with a single wire.

orientations/shapes using different self-assembly methods^{5–9,15–16}. For example, several groups demonstrated control over the growth rate of each crystallographic plane by adding charged complex ions or metal ions, affecting surface properties and nucleation, through solution-based growth^{6–7,17–19}. They only achieved to obtain wires with controlled aspect ratios and morphology, but the possibility for controlled growth in polar and non-polar orientation was not demonstrated. On the basis of the conventional epitaxial growth technique, control of the growth orientation including polar and non-polar directions was achieved by using appropriately selected or engineered single-crystal substrates^{2,8}. However, these approaches require sophisticated techniques and/or particular substrates with specific thermal expansion coefficient, rotational symmetry, and lattice constants. These are of serious impediments to the extension to a large variety of compound semiconductors because of considerable complexities and difficulties in engineered substrate preparation and in finding perfect material-substrate matches from a limited number of epitaxial relationships. Furthermore, other strategies based on a vapor-liquid-solid process were developed using the assistance of either self or foreign catalysts^{5,9,10,15,16,20}. However, the deterministic control of crystal growth is still a challenge due to the presence of various competing precipitation and nucleation behaviors at the liquid-solid interface and the lack of basic understanding of synthetic processes for facet nucleation and growth^{5,9,10,15,16,20}. Therefore, it is

highly necessary to seek for a novel and simple strategy for realizing the facet tailoring.

To this end, we focus on the general and fundamental principle that the surface energy can be mediated by the electron configuration associated with surface states. This enables us that the preferred growth orientation and the crystal shape can be transformed by modifying the electrostatic energies of the surface. For this study, we chose ZnO as a typical wurtzite semiconductor, because this material has the richest family of structures and diverse functionalities, yet to date, no reports have demonstrated precise control over crystallographic orientations and facets of 1D ZnO structure.

Figure 1a shows conceptual schematics of different growth directions with distinct geometric properties and a possible scenario where surface substitutional atoms enable the modulation of surface energy with the expectation of changing the growth directions of ZnO wires. As is well known from previous results reported by other groups^{21,22}, calculations show that for pure ZnO the surface energy of the polar $(000\bar{1})$ plane is much larger than that of the non-polar $(10\bar{1}0)$ and $(11\bar{2}0)$ planes (Supplementary Figure S1). This leads to a polar growth direction with equivalent non-polar side facets with hexagonal symmetry, which are low-index crystallographic planes and low-energy surfaces (as depicted in the left of Figure 1a). In contrast, the polar surface can be made more stable than the non-polar surfaces by replacing surface Zn atoms with Ga atoms. This



implies that a Ga atom could be an attractive foreign species to allow the electrostatic energy gain at the polar surface, resulting in lowering of surface energy of the said plane. Hence, ZnO wires having diamond or rectangular cross sections can be grown preferentially with a polar growth front plane, leaving behind low-energy planes, namely, polar planes to minimize the surface energy, as shown in the right schematic of Figure 1a (also see Supplementary Figure S1). We note that this scheme of surface energy modification for controlled growth could be generalized and extended to various other types of semiconducting materials.

In order to demonstrate controlled crystallographic growth of ZnO wires, a vapor phase transport process has been utilized. A single crystalline GaAs wafer was employed as a Ga source to keep a stable Ga flux at a high growth temperature under Ar ambient. The controlled vapor transport of Ga was maintained during the growth and the relative amount of a Ga flux was controlled by the mass ratio of ZnO and GaAs source materials (see Methods). Figure 1b shows optical microscopy images of usual, ultra-long ZnO wires with lengths of several millimeters grown with the mass ratio of 5 at the temperature of 910°C. Some wires even have lengths longer than 1 cm (Supplementary Figure S2). It is also clearly confirmed that wires are the wurtzite structured ZnO by transmission electron microscopy (TEM) observations (selected area electron diffraction (SAED, Figure 1c) and energy dispersive spectroscopy mapping (EDS, Figure 1d)) and X-ray diffraction (XRD) measurements (Supplementary Figure S2) based on structural and elemental analysis.

Control of the geometrical morphology of ZnO wires was achieved by adjusting the relative amount of GaAs source material, shown in the high-magnification scanning electron microscopy (SEM) images in Figures 1e–g (also see Supplementary Figure S3). As the relative amount of GaAs sources increases, the morphology of ZnO wires is transformed from a hexagonal cross-section shape (Figure 1e), which is a typical manifestation of the six-fold crystallographic symmetry along the polar direction, to a diamond (Figure 1f) and a rectangular (Figure 1g) cross-sectional shape consisting of distinctly different characteristic orientations. A comparison of the Micro-Raman spectroscopy and secondary ion mass spectroscopy (SIMS) results obtained from wires with a non-hexagonal cross-section clearly confirm the incorporation of Ga atoms (Figures 1h and S4a). Figure 1i shows survey spectra obtained from near the surface (marked “A”) and centre (marked “B”) of a single wire by field emission Auger electron spectroscopy (FE-AES) with good spatial resolution and good sensitivity for a wide range of elements, exhibiting that the amount of Ga atoms was less than the detectable range. The X-ray photoelectron spectroscopy (XPS) results (Supplementary Figure S4c) also show the absence of Ga-related alloys or precipitates in ZnO wires. In addition to demonstrating the controlled growth of ZnO wires by the introduction of GaAs source materials, we have also achieved similar control over the morphology and shape of ZnO wires by using pure Ga source materials (see Supplementary Figure S4b). These findings demonstrate that crystal shape and growth direction of ZnO are directly affected by Ga species. Crystal growth typically occurs normal to the plane with high surface energy, in order to minimize the total surface energy. This implies that the bounding facets of ZnO wires formed during the growth have lower energy surfaces compared to the growth front plane of ZnO.

To clearly verify the growth direction and crystal structure of ZnO wires with different morphologies, TEM samples were prepared by cross-sectioning a wire using a focused ion beam. Figure 2 shows cross-sectional TEM images taken from individual wires and the corresponding SAED patterns. A SAED pattern of a hexagonal-shaped ZnO wire taken along the $[0001]$ zone axis, which is parallel to the vertical direction of its cross-section, indicates a single crystalline wurtzite structure of a wire grown preferentially along the $[0001]$ direction as shown in Figure 2a. It can be also seen that a hexagonal-shaped wire is enclosed by equivalent $\{01\bar{1}0\}$ planes and

that the angles between bounding side facets are either 60 or 120°. In contrast, however, for a diamond- and a rectangular-shaped ZnO wire shown in Figures 2b and c, respectively, it is found that wires have the non-polar $[1\bar{1}00]$ and $[2\bar{1}10]$ growth directions and are enclosed by $\{11\bar{2}4\}$ and $\{1\bar{1}2\bar{4}\}$ side facets and $\{0001\}$ and $\{0\bar{1}10\}$ side facets forming diamond and rectangular cross sections, respectively. In addition, the structural orientations between bounding side planes are in excellent agreement with measured values from low-magnification TEM images and SAED patterns. Also, high-resolution TEM images of cross-sections of non-hexagonal shaped wires clearly show (0001) lattice fringes, further confirming that wires grow along the non-polar direction parallel to a polar (0001) plane (It should be noted that a few wires grown along a polar direction exhibit a diamond cross-section consisting of four equivalent $\{02\bar{2}\bar{2}\}$ side planes as shown in Figure S5).

To further understand the role of GaAs in determining the shape and growth direction of ZnO wires, we performed density functional calculations (see Methods for details). It is found that pure ZnO slabs with top (0001) and bottom (000 $\bar{1}$) surfaces, which are regarded as the most unstable surface, have surface cleavage energy of 3.92 J/m². This is much higher than that of other slabs with non-polar (10 $\bar{1}0$) and (11 $\bar{2}0$) surfaces, which is 2.01 and 2.03 J/m², respectively. These values are in good agreement with previous calculations^{21,22}. However, when Ga atoms replace surface Zn atoms with a half monolayer (ML) coverage, the corresponding change of surface energy ($\Delta\gamma$) calculated at (0001), (000 $\bar{1}$), (10 $\bar{1}0$), and (11 $\bar{2}0$) surfaces is significantly altered, as summarized in Figure 3a (also see Tables S1 and 2 and Figures S1 and 6a). Surface energy at the O-terminated (000 $\bar{1}$) surface is significantly lowered by 1.85 J/m², while the surface energy at (0001), (10 $\bar{1}0$), and (11 $\bar{2}0$) surfaces is increased by 0.07, 0.80, and 0.90 J/m², respectively. In addition, here, we propose the surface energy lowering mechanism to elucidate that the large reduction of surface energy at the O-terminated surface by Ga addition can be explained in terms of the electron-counting rule (ECR)^{23,24}. When Ga atoms replace surface Zn atoms at a half ML coverage, additional electrons at high-energy Ga 4p states fully fill the low-energy dangling bond states of surface O atoms, allowing the electrostatic energy gain and thereby lowering the surface energy (Figure S6b).

Figure 3b shows the calculated surface band structures of a clean and a Ga-incorporated (000 $\bar{1}$) surface. As discussed and shown schematically in Figure S6b, the surface oxygen states are partly empty in the clean surface (the left in Figure 3b), while for the Ga-incorporation in the clean surface (the right in Figure 3b), the surface states are fully filled in accordance with the ECR. Moreover, the calculated band structure shows that the energy levels of the surface states are decreased by ~ 1 eV owing to the electrostatic interaction with more positive Ga ions. This also accounts partly for the high surface energy gain by Ga substitution. Additionally, As atoms might be also incorporated on the ZnO surface during the growth by replacing surface O atoms, which nominally satisfies the ECR. However, this results in removal of electrons in the surface states near the valence band edge, and thus it is hard to expect the energy gain. Also, because of the reduced electronegativity of As atoms and larger atomic size of As compared to O atoms, resulting in the steric hindrance and structural distortion, the surface bands become very unstable (Figures S7 and 8) and the surface energy increases significantly. Thus, the surface energy lowering by Ga incorporation at the O-terminated surface is expected to be the main driving force for the growth of the ZnO wires with a polar direction, because it is expected theoretically that the incorporation of As atoms does not change the growth mode by changing surface energy ordering.

In order to address whether our approach can be generalized, we performed further calculations with group III elements, being expected to allow similar effects on the electrostatic energy gain to Ga atoms. In fact, it is found that the incorporation of group III elements can give a much higher energy gain at the polar (000 $\bar{1}$)

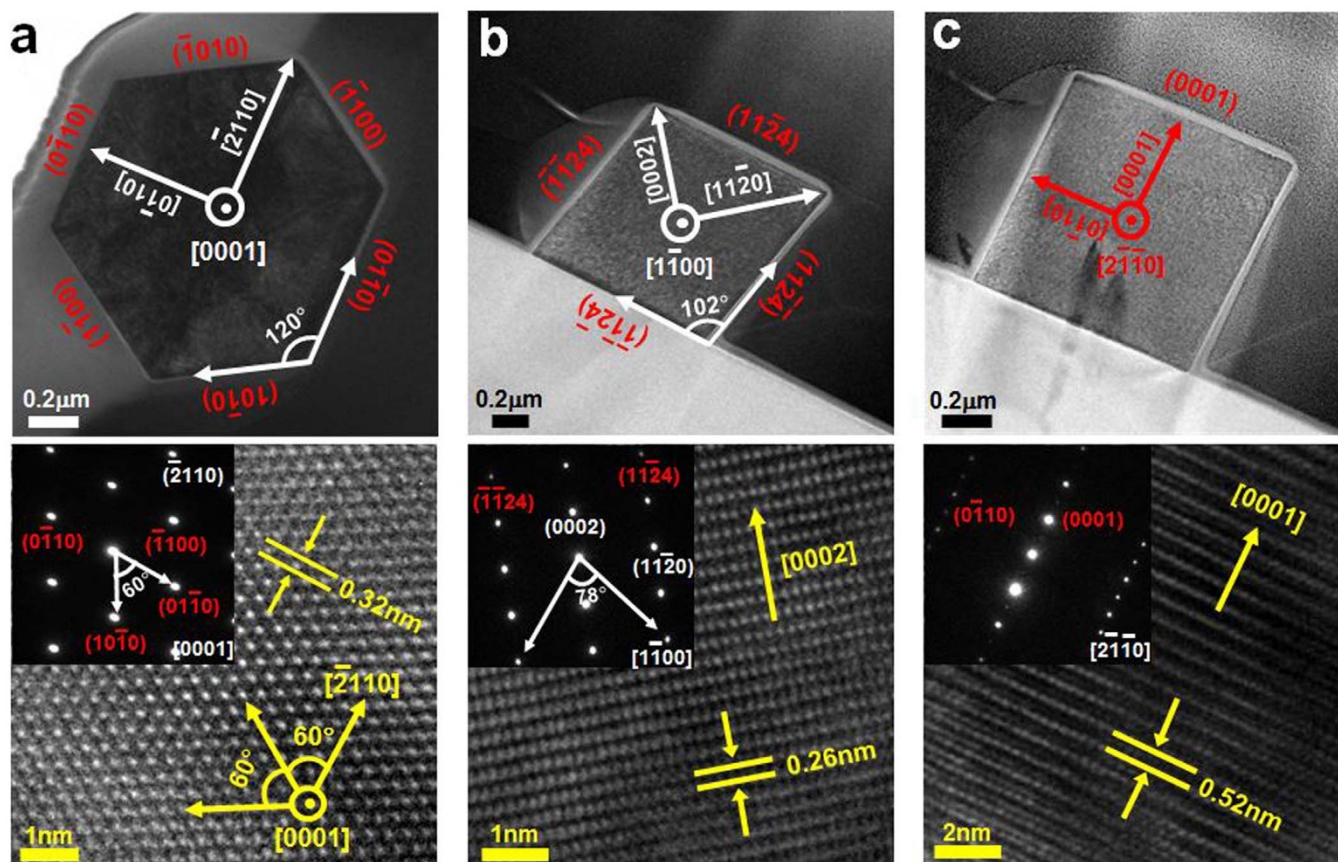


Figure 2 | TEM images of ZnO wires: Cross-sectional TEM images, and high-resolution TEM images of ZnO (columns 1–2, top to bottom). (a), ZnO wires with a hexagonal cross-section. A high-resolution TEM image obtained from a cross-section of a wire and the corresponding SAED pattern indexed to wurtzite ZnO show that a wire grows along a polar $[0001]$ direction parallel to non-polar $\{01\bar{1}0\}$ side planes. (b–c), ZnO wires with diamond (b) and rectangular (c) cross-sections, respectively. The corresponding SAED patterns HRTEM images indicate that wires can be preferentially grown with the non-polar $[1100]$ and $[2\bar{1}10]$ directions.

surface compared with other surfaces, as summarized in Figure S9a. Similar to Ga atoms achieved for the growth of ZnO wires along non-polar directions, we have also achieved similar control over the

growth orientation of ZnO wires by modulating surface energy with Al elements due to the relatively large surface energy lowering (see Supplementary Figure S9b). It has been reported that additional

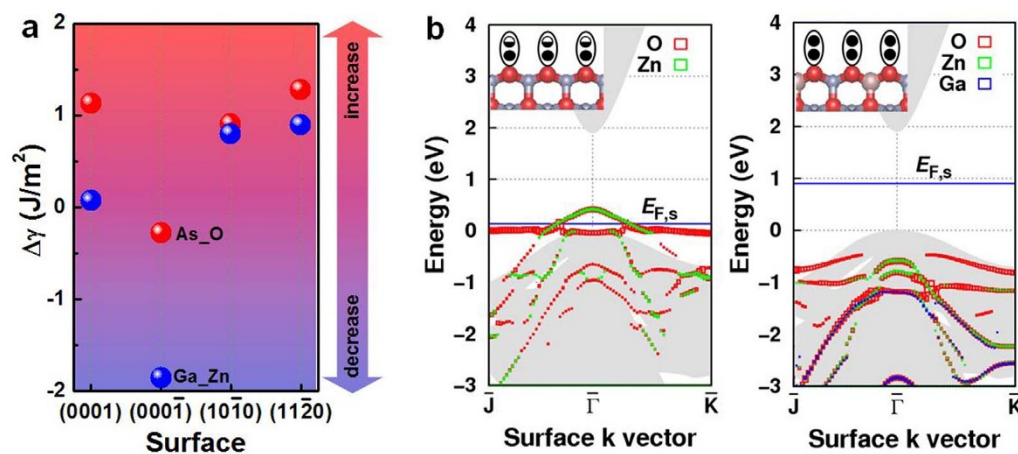


Figure 3 | Electronic structure calculations. (a), Surface energy change before and after the introduction of surface substitutional atoms at various surfaces. The calculated results show that the polar surface energy becomes significantly lower than non-polar surfaces when Ga atoms replace surface Zn atoms at a half monolayer coverage. (b), Calculated surface band structures of clean (left) and Ga-incorporated (right) $(000\bar{1})$ surfaces. (The left inset) The oxygen dangling bonds at the bare (1×1) surface have one and half electrons and thus have a half vacancy. (The right inset) Ga substitutional atoms at a half monolayer coverage make the dangling bonds fully filled. In addition, it is found that the energy levels of the surface states are decreased by ~ 1 eV. The reference bulk bands are denoted by grey colors and the surface states are denoted by red, green, and blue depending on the contribution from surface O, Zn, and Ga atoms, respectively.

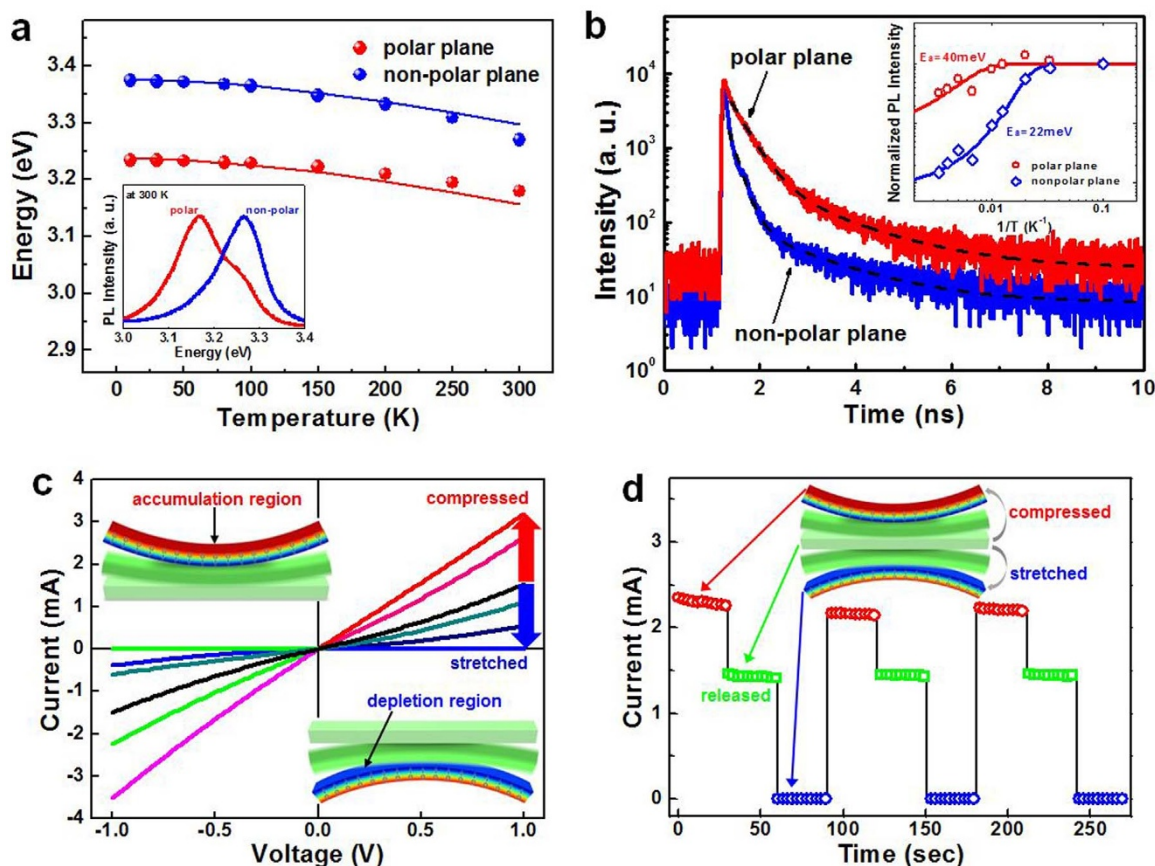


Figure 4 | Effects of the polarization field on optical and electrical characteristics of ZnO wires. (a), Temperature-dependent PL emission energy of ZnO wires grown in polar (filled blue circles) and non-polar (filled red circles) directions. The fitting lines are plotted using Varshni's relation. The inset shows representative room-temperature, single wire PL spectra obtained from ZnO wires with controlled orientations. (b), Time-resolved PL properties of selectively grown ZnO wires with different crystallographic orientations. These results reveal that the polar plane exhibits the prolonged decay time compared to the electrostatic field-free plane. The inset shows temperature dependence of normalized intensity of emissions related to polar (red) and non-polar (blue) planes. (c), Electrical characteristics of a single ZnO wire with a non-polar growth direction perpendicular to the *c*-axis. Note that positive or negative polarization is uniformly induced on the wire surface along the length because the polarization field is generated in the direction of the *c*-axis, causing modulation in channel conductance. In the inset, the color gradient indicates the piezoelectric potential distribution where the red and blue color presents the positive and negative piezoelectric potential, respectively. (d), Switching characteristics of a two-terminal device measured with $V_{DS} = 1$ V, clearly showing that channel conductance is reproducibly changed after the application of compressed and stretched stresses, respectively. The inset indicates the corresponding piezoelectric potential to wires being bent upwards/downwards.

charged complex ions or Ga ions in the growth solution strongly affect the morphology, size, and aspect ratios of ZnO wires^{6,17–19}. However, they only demonstrated to control wire morphology, not to alter the growth direction due to the low-temperature growth process, which is mainly governed by kinetics rather than thermodynamics. Thus, it is important to note that our finding and growth-control mechanism are distinct from results reported previously in solution-based approaches under complex ions or Ga ions assistance^{6,17–19}.

The ability to control the crystallographic orientation and morphology of anisotropic ZnO wires enables us to achieve the designed physical properties because the presence of spontaneous and piezoelectric polarization strongly influences the behaviors of excitons and electron-hole overlap associated with optical characteristics^{1,2}. In order to demonstrate such a surface polarity effect on photophysical properties, we conducted temperature-dependent micro-photoluminescence (PL) measurements with a spatial resolution of 1 μm , which can assess individual surface facets within a single wire. Figure 4a shows a clear difference in the emission energy from polar and non-polar crystallographic orientations of ZnO wires at temperatures ranging from 10 K to 300 K. The optical emission from the polar plane is red-shifted by 100–120 meV as compared with wires

consisting of non-polar planes. As ZnO wires have similar length and diameter as shown in SEM and TEM results (Figures 1 and 2), the difference in the evolution of PL spectra between the two sets of samples is attributed to the electrostatic field induced by the spontaneous polarization associated with crystallographic side surfaces and growth directions. This optical behavior of ZnO wires is consistent with the evolution of cathodoluminescence (CL) spectra (Figure S10), which show different emission from the polar surface compared to the non-polar surface, with a shift towards lower transition energy. For nitride-based semiconductors the spontaneous polarization-induced electrostatic field results in the transition energy shifts^{1,2}, which suggests that the energy shift in the polar plane of a ZnO wire is mainly caused by the localized electrostatic field.

Time resolved PL measurements were carried out using a frequency tripled Ti:sapphire laser (266 nm, 150 ps) and fitted with two exponentials (Figure 4b). The polar plane exhibits a longer decay time (711 ps) compared to the electrostatic field-free plane (584 ps), indicating another direct manifestation of the presence of the electrostatic field in ZnO wires grown along the non-polar direction. It is also found that the activation energy of a polar plane, obtained from normalized PL intensity, is higher than that of non-polar plane by 18 meV (the inset of Figure 4b)²⁵. These differences in emission



energy, luminescence decay time, and activation energy, show how the spontaneous polarization in a ZnO wire can affect the optical properties. This paves the way to tailoring the exciton lifetime of ZnO for specific optoelectronic devices, where long exciton lifetimes are desired for photovoltaic devices and short lifetimes for light-emitting diodes, photodetectors, and high luminous efficiency displays.

Another material property of anisotropic semiconductors, depending on their crystallographic orientations coupled with the spontaneous polarity and piezoelectricity, is the carrier concentration and charge density. For the utilization of these attractive features in electronic devices, inducing the uniform polarization along the semiconducting channel surface would be crucial for an effective polarization field effect on the channel conductance. For this, we fabricated two-terminal devices based on a ZnO wire having a non-polar $[2\bar{1}\bar{1}0]$ growth direction with a polar side surface and then investigated their electrical transport characteristics. We observed reversible and reproducible modulation in channel conductance (more than 3 orders of magnitude) by bending a wire upwards or downwards (figure 4c). ZnO has the largest piezoelectricity along its polar c -axis crystal direction. In a conventional ZnO wire with polar growth direction the polarization field is induced parallel to the wire length, whereas in ZnO wires with non-polar growth direction the piezoelectric polarization is induced perpendicular to the polar axis, i.e. along the length of the wire surface. Compressive (tensile) stress is induced on the channel surface when we bend the ZnO wire with a non-polar orientation downwards (upwards). This results in the positive (negative) piezoelectric potential uniformly along on the wire surface as shown in the top left inset of Figure 4c (the bottom right inset of Figure 4c), which causes the accumulation (depletion) of electrons in the channel. Consequently, this resulted in an increase (decrease) in the channel conductance. We also demonstrate the reversible switching of the three different conductance states, defined as the compressed (high conductance), the released (initial conductance), and the stretched (low conductance) states of two-terminal devices (Figure 4d). The three stable states were continuously measured at $V_{DS} = 1$ V and reproducibly switched by the application of compressed and stretched stresses. These results indicate that the large modulation of channel conductance mainly originates from the nature of the piezoelectric polarization uniformly induced on the wire surface along the length. Here, it is important to note that our ZnO wires with controlled orientation did not seem to be significantly altered in their intrinsic material properties, such as, structural, optical, and electrical properties, as confirmed by XRD (Supplementary Figure S2a), TEM (Figure 2), and PL measurements (Figure 4a) as well as electrical characterizations (Figure 4c) due to the limited bulk incorporation, being the basis of modest defect sites (see Supplementary Figure S6). Thus, this suggests a new topology of piezoelectric devices which are totally different from conventional ones with the piezoelectric field in the direction of wire length modulating a local Schottky barrier height^{26,27}.

We have shown that Ga ions can be used to modulate the surface energy of ZnO crystal facets during growth and provide control over the crystal growth direction of anisotropic wires. Characterization revealed the optical and piezoelectric properties were highly dependent upon crystal structure of the ZnO wires. Our approach for the surface polarity-selective growth should be generic for wurtzite semiconducting materials and provides new opportunities for their implementation as functional materials in optical, photonic, piezoelectric and electrical devices.

Methods

Synthesis. ZnO wires were thermally grown using a vapor phase transport process by vaporizing ZnO:C mixed powder (weight ratio ZnO:C = 1 : 1) and GaAs powder. The wires were grown without employing any metal catalysts and collected at top of an alumina boat (Supplementary Figure S2) inserted into a quartz reaction tube, which was placed in the middle of a high temperature tube furnace. Prior to the growth, the alumina tube was first purged by Ar gas for 10 min and then the furnace was heated at

a rate of 30°C/min. The growth temperature and time were 910°C and 30 min, respectively. The weight ratio of source powder ((ZnO + C)/GaAs) have been controlled from 2 to 20 with respect to 50 mg of (ZnO + C) power, which is an important control parameter for achieving the designed crystal growth of ZnO wires.

Modeling. Our first-principles calculations are based on the density functional theory (DFT) employing the generalized gradient approximation (GGA) and the projector-augmented-wave method as implemented in VASP^{28–30}. Valence electronic wave functions are expanded in a plane wave basis set with a cutoff energy of 400 eV. The equilibrium lattice parameters for wurtzite ZnO are calculated to be $a = 3.151$ Å, $c = 5.068$ Å, and $u = 0.380$, compared to experimental values of $a = 3.250$ Å, $c = 5.207$ Å, and $u = 0.383$ (Here u is the bond length of vertical Zn–O bonds, normalized by c). Surface cleavage energies are calculated with periodic slabs, with slab thickness of 2–3 nm and vacuum spacing of ~ 10 Å. The k -point integration over the surface Brillouin zone uses mesh spacing of ~ 0.31 Å⁻¹. The atomic positions are relaxed until residual forces are less than 0.02 eV/Å. The band gap underestimation of the GGA scheme is partly corrected ($E_g = 1.90$ eV) by adopting the GGA + U scheme with an onsite Coulomb repulsion parameter U of 8 eV for the Zn d -orbitals³¹.

When Ga atoms are introduced to replace Zn on the surface, the surface energy change ($\Delta\gamma$) is given as

$$\Delta\gamma = \frac{1}{A} \{E_{tot}(Ga_{Zn}) - [E_{tot}(\text{clean}) - n_{Zn}\mu_{Zn} + n_{Ga}\mu_{Ga}]\}$$

where $E_{tot}(\text{clean})$ and $E_{tot}(Ga_{Zn})$ are the total energies of clean and Ga-incorporated ZnO slabs, respectively. n_{Zn} and n_{Ga} are the respective number of removed Zn and added Ga atoms in the surface area A . The chemical potential of Ga, μ_{Ga} , is taken from a Ga metal corresponding to the Ga-rich condition. Similarly the Zn-rich condition is taken for μ_{Zn} .

1. Waltereit, P. *et al.* Nitride semiconductors free of electrostatic field for efficient white light-emitting diodes. *Nature* **406**, 865–868 (2000).
2. Kuykendall, T. *et al.* Crystallographic alignment of high-density gallium nitride nanowire array. *Nat. Mater.* **3**, 524–528 (2004).
3. Han, X. *et al.* Strain-gradient effect on energy band in bent ZnO microwires. *Adv. Mater.* **3**, 4707–4711 (2012).
4. Liao, Z. *et al.* Strain induced exciton fine-structure splitting and shift in bent ZnO microwires. *Scientific Reports* **2**, DOI:10.1038/srep00425 (2012).
5. Pan, Z. W., Dai, Z. R. & Wang, Z. L. Nanobelts of semiconducting oxides. *Science* **291**, 1947–1949 (2001).
6. Joo, J., Chow, B. Y., Prakash, M., Boyden, E. S. & Jacobson, J. M. Face-selective electrostatic control of hydrothermal zinc oxide nanowire synthesis. *Nat. Mater.* **10**, 596–601 (2011).
7. Tian, Z. R. *et al.* Complex and oriented ZnO nanostructures. *Nat. Mater.* **2**, 821–826 (2003).
8. Tsvion, D., Schwartzman, M., Popovitz-Biro, R. & Joselevich, E. Guide growth of millimeter-long horizontal nanowires with controlled orientations. *Science* **333**, 1003–1007 (2011).
9. Fan, H. J. *et al.* Vapour-transport-deposition growth of ZnO nanostructures: switch between c -axial wires and a -axial belts by indium doping. *Nanotechnology* **17**, s231–s239 (2006).
10. Wang, Z. L. Zinc oxide nanostructures: growth, properties and applications. *J. Phys.: Condens. Matter.* **16**, R829–R858 (2004).
11. Wang, Z. L. Progress in piezotronics and piezo-phototronics. *Adv. Mater.* **24**, 4632–4646 (2012).
12. Yang, Y. *et al.* Thermoelectric nanogenerators based on single Sb-doped ZnO micro/nanobelts. *ACS Nano* **6**, 6984–6989 (2012).
13. Hu, Y. *et al.* Piezo-phototronic effect on electroluminescence properties of p -type GaN thin films. *Nano Lett.* **12**, 3851–3856 (2012).
14. Cha, S. *et al.* Sound-driven piezoelectric nanowire-based nanogenerators. *Adv. Mater.* **22**, 4726–4730 (2010).
15. Gao, H., Ji, H., Zhang, X., Lu, H. & Liang, Y. Indium-doped ZnO nanospirals synthesized by thermal evaporation. *J. Vac. Sci. Technol. B* **26**(2), 585–588 (2008).
16. Wang, Z. L. ZnO nanowire and nanobelt platform for nanotechnology. *Mater. Sci. Eng. R* **64**, 33–71 (2009).
17. Park, G. C., Hwang, S. M., Lim, J. H., & Joo, J. Growth behavior and electrical performance of Ga-doped ZnO nanorod/ p -Si heterojunction diodes prepared using a hydrothermal method. *Nanoscale* **6**, 1840–1847 (2004).
18. Pineda-Hernandez, G., Escobedo-Morales, A., Pal, U. & Chigo-Anota, E. Morphology evolution of hydrothermally grown ZnO nanostructures on gallium doping and their defect structures. *Mater. Chem. Phys.* **135**, 810–817 (2012).
19. Wang, H., Baek, S., Song, J., Lee, J. & Lim, S. Microstructural and optical characteristics of solution-grown Ga-doped ZnO nanorod arrays. *Nanotechnology* **19**, 075607 (2008).
20. Yuan, G.-D. *et al.* Tunable n -type conductivity and transport properties of Ga-doped ZnO nanowire arrays. *Adv. Mater.* **20**, 168–173 (2008).
21. Na, S & Park, C. First principles study of the surface of wurtzite ZnO and ZnS – Implication for nanostructure formation. *J. Korean Phys. Soc.* **54**, 867–872 (2009).
22. Wander, A. *et al.* Stability of Polar Oxide Surfaces. *Phys. Rev. Lett.* **86**, 3811–3814 (2001).



23. Pashley, M. D. Electron counting model and its application to island structures on molecular-beam epitaxy grown GaAs(001) and ZnSe(001). *Phys. Rev. B* **40**, 10481–10487 (1989).
24. Harrison, W. A. Theory of polar semiconductor surfaces. *J. Vac. Sci. Technol.* **16**, 1492–1496 (1979).
25. Leroux, M. *et al.* Temperature quenching of photoluminescence intensities in undoped and doped GaN. *J. Appl. Phys.* **86**, 3721–3728 (1999).
26. Zhang, Y., Liu, Y. & Wang, Z. L. Fundamental Theory of Piezotronics. *Adv. Mater.* **23**, 3004–3013 (2011).
27. Yu, R. *et al.* Piezotronic effect on the transport properties of GaN nanobelts for active Flexible electronics. *Adv. Mater.* **24**, 3532–3537 (2012).
28. Perdew, J. P., Burke, K. & Ernzerhof, M. Generalized gradient approximation made simple. *Phys. Rev. Lett.* **77**, 3865–3868 (1996).
29. Kresse, G. & Furthmuller, J. Efficient iterative schemes for ab initio total-energy calculations using a plane-wave basis set. *Phys. Rev. B* **54**, 11169–11186 (1996).
30. Kresse, G. & Joubert, D. From ultrasoft pseudopotentials to the projector augmented-wave method. *Phys. Rev. B* **59**, 1758–1775 (1999).
31. Liechtenstein, A. I., Anisimov, V. I. & Zaanen, J. Density-Functional Theory and Strong Interactions: Orbital Ordering in Mott-Hubbard Insulators. *Phys. Rev. B* **52**, R5467–R5470 (1995).

Acknowledgments

This work was supported by the Korea Institute of Energy Technology Evaluation and Planning (KETEP) (20128510010080, 20138520030800). W.-K.H. acknowledges the financial support from the Korea Basic Science Institute (KBSI) (no. T34516) and the

NRF-BC Researcher Links through the National Research Foundation of Korea (NRF) funded by the Ministry of Science, ICT and future planning (no. NRF-2013K2A1C1076556).

Author contributions

J.I.S., W.-K.H. and S.C. carried out experimental design, device fabrication and data analyses. S.L. and J.K. carried out simulations and data analyses. S.L. carried out the device measurement. Y.J.P., J.H., S.H., J.H.W. and K.H.P. contributed to the scientific discussion. J.M.K. planned and designed the work and provided experimental guidance. J.I.S., J.H.W. and S.C. wrote the manuscript.

Additional information

Supplementary information accompanies this paper at <http://www.nature.com/scientificreports>

Competing financial interests: The authors declare no competing financial interests.

How to cite this article: Sohn, J.I. *et al.* Surface energy-mediated construction of anisotropic semiconductor wires with selective crystallographic polarity. *Sci. Rep.* **4**, 5680; DOI:10.1038/srep05680 (2014).



This work is licensed under a Creative Commons Attribution-NonCommercial-ShareAlike 4.0 International License. The images or other third party material in this article are included in the article's Creative Commons license, unless indicated otherwise in the credit line; if the material is not included under the Creative Commons license, users will need to obtain permission from the license holder in order to reproduce the material. To view a copy of this license, visit <http://creativecommons.org/licenses/by-nc-sa/4.0/>